Journal of Power Sources 212 (2012) 35–42

Contents lists available at SciVerse ScienceDirect

Journal of Power Sources

journal homepage: www.elsevier.com/locate/jpowsour

# Effects of embossing structure on the performance of intermediate-temperature solid oxide fuel cells with gadolinium-doped ceria electrolyte

Jiho Lee [a], Inyu Park [a], Hunhyeong Lee [b], Dongwook Shin [a,b,*]

[a] Department of Fuel Cells and Hydrogen Technology, Hanyang University, 222 Wangsimni-ro, Seongdong-gu, Seoul 133-791, Republic of Korea
[b] Division of Material Science & Engineering, Hanyang University, 222 Wangsimni-ro, Seongdong-gu, Seoul 133-791, Republic of Korea

ARTICLE INFO

*Article history:*
Received 21 January 2012
Received in revised form
15 March 2012
Accepted 17 March 2012
Available online 9 April 2012

*Keywords:*
Solid oxide fuel cells
Gadolinium-doped ceria
Electrostatic slurry spray deposition
Interfacial resistance
Embossing
Powder ball

ABSTRACT

Using the powder-ball generation phenomenon in the electrostatic slurry spray deposition (ESSD), the embossing structures are introduced on the gadolinium-doped ceria (GDC) electrolyte to expand the cathode–electrolyte interface and three phase boundary. To verify the influence of embossing structure, the half and single cells composed of the GDC electrolyte and $La_{0.6}Sr_{0.4}Co_{0.2}Fe_{0.8}O_{3-\delta}$ (LSCF) cathode are fabricated by the ESSD. The half cell with embossing deposited for 30 s (8.6% of electrolyte surface coverage) shows the lowest cathode polarization resistance, which is lower than that of the half cell without embossing by 62.3%. For the single cells, the maximum power densities are estimated to 0.171 W $cm^{-2}$ and 1.06 W $cm^{-2}$ for the cell without embossing and 0.232 W $cm^{-2}$ and 1.19 W $cm^{-2}$ for the cell with embossing at 550 °C and 750 °C, respectively. Additionally, the open circuit voltage (OCV) is increased by 2–5% at 550–750 °C range. According to the half and single cell results, it may be concluded that the maximum power densities and OCVs of the single cells with embossing increase simultaneously and this improvement is more effective in lower temperature range.



## 1. Introduction

Today, the solid oxide fuel cells (SOFCs) are already commercialized using yttria-stabilized zirconia (YSZ) electrolyte, lanthanum strontium manganate (LSM) cathode, and Ni–YSZ composite (anode). Nevertheless, the efforts to improve the performance and lowering operation temperature of SOFCs have continued by decreasing the electrolyte thickness [1–4] or changing the electrolyte materials such as gadolinium-doped ceria (GDC). Another approach is developing some novel architecture such as the 3-D dome and 1-D nanofiber structures [5,6]. However, the complicated process and several organic additives are required to develop these new architectures. Thus, among these above mentioned efforts, the attempts to optimize or improve microstructure have been widely employed in many researches. Typical examples of these efforts are the anode functional layer [5–7] or cathode functional layer [8–11]. Other than these approaches, the modification of cathode–electrolyte interface morphology by an embossing structure is one of the popular approaches to improve the performance of SOFCs. This embossing structure by the electrolyte surface modification approach aims the expanding interface area. The modified embossing structure on the electrolyte surface could act as the expanded dimension of the cell, but actually small area same as the cell with flat electrolyte surface. Thus, the active triple phase boundary (TPB) between the cathode and electrolyte could be enlarged by the electrolyte surface modification. Although this kind of approach has been already tried several researches [12–14], previous trials used relatively large structural elements of tens or hundreds of micrometers. When the large embossing structures are formed on the electrolyte, the electrolyte ohmic resistance may increase and unintended adverse effects might be produced in the overall cell performance. For this reason, in this paper, the micro size (3–5 μm) 'powder-balls' were introduced to fabricate the embossing structures on the electrolyte surface.

The micro-sized powder-balls were deposited by electrostatic slurry spray deposition (ESSD) to modify electrolyte morphology. We found that various micro scale powder-balls can be easily and rapidly fabricated by controlling of the ESSD processing parameters. In our best knowledge, this phenomenon has never been reported. In addition to this phenomenon, the ESSD method has many advantages over conventional deposition techniques, such as a simple set-up, inexpensive source materials, processing in an ambient atmosphere, and, especially, versatile and convenient control of microstructure [15,16]. Since the ESSD employs

* Corresponding author. Division of Material Science & Engineering, Hanyang University, 222 Wangsimni-ro, Seongdong-gu, Seoul 133-791, Republic of Korea. Tel.: +82 2 2220 0503; fax: +82 2 2220 4011.
*E-mail address:* dwshin@hanyang.ac.kr (D. Shin).

0378-7753/$ – see front matter © 2012 Elsevier B.V. All rights reserved.
doi:10.1016/j.jpowsour.2012.03.078

the powder slurry including solid particles, the porous or dense layers as well as powder-balls can be fabricated and the whole cell fabrication is possible with the ESSD method. Therefore, the ESSD method was used not only to modify the electrolyte surface morphology but also to fabricate the cathode and electrolyte layers of the cells studied in this work.

Unlike, the previous trials employing YSZ electrolyte and LSM cathode [12–14], GDC electrolyte and $Ba_{0.5}Sr_{0.5}Co_{0.8}Fe_{0.2}O_{3-\delta}$ (BSCF) and $La_{0.6}Sr_{0.4}Co_{0.2}Fe_{0.8}O_{3-\delta}$ (LSCF) mixed ionic-electronic conductors (MIECs) were employed in this work. This cell structure is certainly aiming intermediate-temperature solid oxide fuel cells (IT-SOFCs), in which more effective performance enhancement by embossing structure is needed.

In this paper, it has been confirmed that the embossing structures can be fabricated by the powder-balls deposition on the electrolyte, and the overall cell performance were greatly improved by this structure.

## 2. Experimental

The whole fabrication processes for half cells and single cells were carried out by the ESSD method, except the process for preparing starting substrates. To fabricate GDC based half cells, the 1.0 g GDC powder (Fuel Cell Materials, USA) was uni-axially pressed (20 MPa, for 5 s) in the 21 mm diameter stainless steel mold, and sintered at 1400 °C in air for 2 h. The obtained dense GDC pellets were 16 mm in diameter and 0.7 mm in thickness. The GDC embossing structures were formed on the obtained GDC pellets by ESSD method. The GDC slurry applied to the formation of the powder-balls was prepared with GDC powder, Isopropyl alcohol (IPA, Daejung, Korea, >99.5%) and Toluene (Daejung, Korea, >99.5%), in the weight ratio of 58.3:25:16.7. To increase dispersion stability of the slurry, the ultra-sonification process was applied for an hour. Subsequently, the powder-balls were deposited onto GDC pellets by the ESSD method with the spray conditions; nozzle-substrate distance of 7 cm, applied voltage of 9 kV, and slurry supply flow rate of 1 mL $h^{-1}$. The deposition time was varied from 15 to 240 s to change the amount of powder-balls. The GDC substrates with embossing structure were produced by sintering this GDC pellets with powder-balls at 1400 °C for 2 h. The 'flat' GDC substrates, without powder-ball deposition, were subjected the identical fabrication and sintering process to produce the same grain structure and eliminate the possible effect of different grain structure in the electrolyte. The porous BSCF (Kceracell, Korea) cathode was also deposited by the ESSD process under the condition; spray distance of 11 cm, applied voltage of 9 kV, flow rate of 5 mL $h^{-1}$, and deposition time of 20 min. BSCF slurry was prepared by the same formula as the GDC slurry, but the weight of powder was reduced to half to produce the porous microstructure of the cathode layer. The as-deposited BSCF cathode was sintered at 900 °C for 2 h.

NiO–GDC anode supported single cells with embossing structure were also fabricated by using the ESSD method. To prepare the NiO–GDC anode substrate, NiO (Daejung, Korea) and GDC powders were weighed 60:40 in wt%, and then carbon-black of 15 wt% was added. The mixed powders were dry ball-milled for 10 h. The prepared composite powders were uni-axially pressed (20 MPa, for 5 s) in the stainless steel mold with the diameter of 25 mm. Subsequently, the GDC electrolyte layer was immediately deposited without anode pre-sintering using the GDC slurry used in the half cell fabrication. The deposition conditions were nozzle-substrate distance 11 cm, applied voltage 9.75 kV, flow rate 10 mL $h^{-1}$, and deposition time 20 min. The powder-balls were sprayed onto the as-deposit electrolyte under the same condition as the half cell fabrication with embossing structures. The deposition time was 30 s, and the un-sintered anode and the electrolyte layer with powder-ball embossing were co-fired at 1450 °C for 3 h. Finally, the LSCF (Fuel Cell Materials, USA) cathode was deposited by the ESSD method, and it was sintered at 1050 °C for 2 h. The slurry preparation and the deposition process for the cathode were conducted with the same ways for the BSCF half cell.

The microstructure and morphology of the prepared cells were observed by scanning electron microscopy (SEM, JEOL JSM-6360). In addition, the surface coverage of embossing structures was obtained by image analysis programs (Image-Pro Plus). For measuring electrochemical property of the half cells, the three-electrode method was used. For single cells, the diluted Pt paste was painted on the cathode and the anode side with the area of 1 $cm^2$. The prepared single cells were mounted on the test rig with a ceramic sealant (516 ceramic bond, Aremco). The flow rate of dry air and wet hydrogen (passed through a humidifier) were 200 sccm. The impedance spectroscopy of the half cells and current–voltage ($I$–$V$) characteristics of the single cells were measured by a frequency response analyzer (Solartron Instruments 1260, UK). Impedance measurements were performed at OCV on the half cells, using a frequency range from $10^6$ Hz to 0.01 Hz and amplitude of 20 mV. $I$–$V$ characteristics were measured using linear sweep voltage, scanning at a rate of 20 mV $s^{-1}$.

## 3. Results and discussion

### 3.1. Performance enhancement in the half cells

The embossing structures were successfully fabricated by the ESSD method and the produced microstructures are shown in Fig. 1 and Fig. 2. Fig. 1(a) and (b) are the tilt and top view of embossing

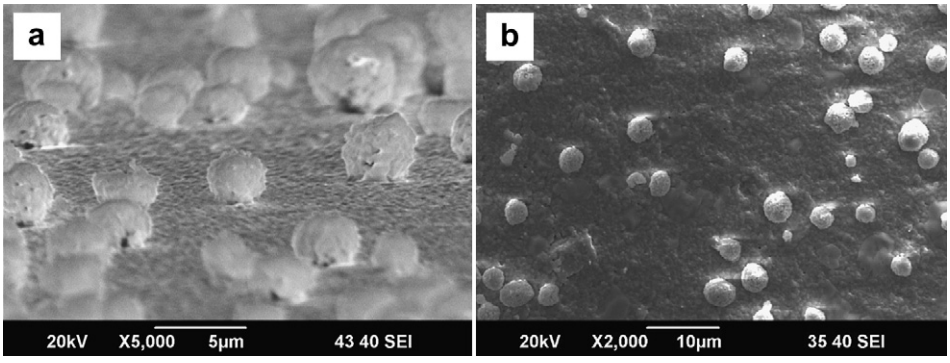


**Fig. 1.** SEM images of GDC embossing structures morphology on GDC electrolyte: (a) tilt and (b) top view of embossing structure sintered at 1400 °C for 2 h.

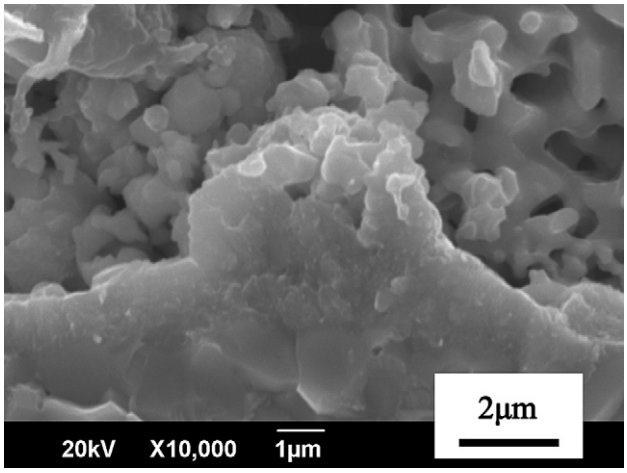


**Fig. 2.** A magnified cross-sectional SEM image of embossing structure produced by a powder-ball.

structures on the electrolyte and Fig. 2 is the cross-sectional images of the embossing structure embedded in the GDC/BSCF half cell. The average size of powder-ball was about 3 μm, and the shape was almost sphere. The formation process of powder-ball in electrospray deposition is schematically summarized in Fig. 3. The sprayed slurry droplets are rapidly split into finer droplets when the specific charge density accumulate in the droplet surface reaches to the 'Rayleigh limit' (the magnitude of charge on a droplet that leads to the droplets fission by overcoming the surface tension force [17]) and the solid particles in the droplets are forced toward inside during the solvent evaporation before landing on the substrate [18,19]. After the solvent completely evaporates, the powder particles agglomerate into ball shape due to physical adhesion. Although the powder-balls do not form chemical bonding with the electrolyte surface right after deposition, the necking between particles could be developed by high temperature sintering as shown in Fig. 2. The spray condition to produce powder-ball is slightly higher spray voltage than stable cone-jet spray condition. At this condition, the sprayed droplets start to become larger due to unstable drop formation [19]. However, at excessively high voltage, the generation of droplet becomes uncontrollable and the size distribution of droplet becomes scattered widely and the deposition becomes non-uniform. Therefore, there is an optimum voltage and, hence, other deposition parameters affecting dielectric environments of deposition chamber have to be controlled to produce this optimum powder-ball generation voltage.

Fig. 4 shows the surface coverage of the deposited powder-balls as a function of deposition time. The deposition time was varied from 15 s to 240 s, and the percentage of surface area covered by the powder-balls (painted dots in Fig. 4(a)–(f)) was gradually increased from about 4.5% to 55.2%. As shown in Fig. 4(g), the surface coverage, $\theta$, of the powder-balls approximately follows the Langmuir isotherm ($\theta = 1 - \exp(-kt)$), which suggests that the powder-ball deposition proceeds almost in monolayer. This monolayer deposition is preferred in the aspect of cell performance since it minimize undesirable increase of electrolyte thickness and, hence, ohmic resistance. Fig. 5 summarizes the variation of total polarization resistances as functions of the deposition time of embossing structures in the GDC/BSCF half cells measured from 550 °C to 750 °C. From the result, it should be noted that the lowest polarization resistance was obtained in the specimen deposited for 30 s in all measuring temperature range, and the polarization resistance increases as the deposition time increases over 30 s. This result suggests that the optimized surface coverage of embossing structures is about 8.6% deposited for 30 s.

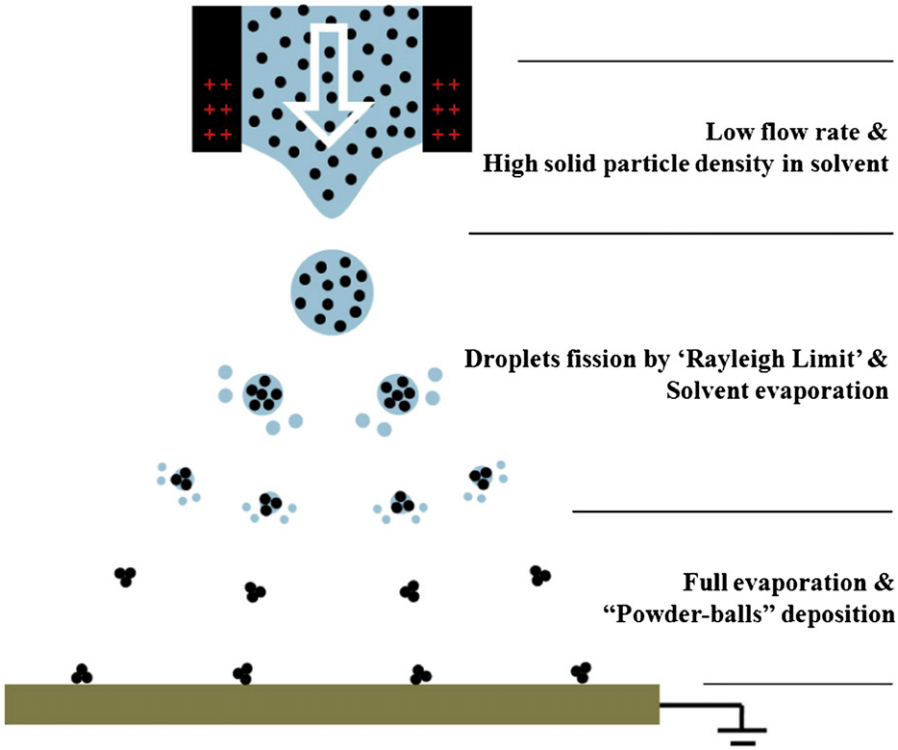


**Fig. 3.** Schematic of the powder-ball generation mechanism by the ESSD method.

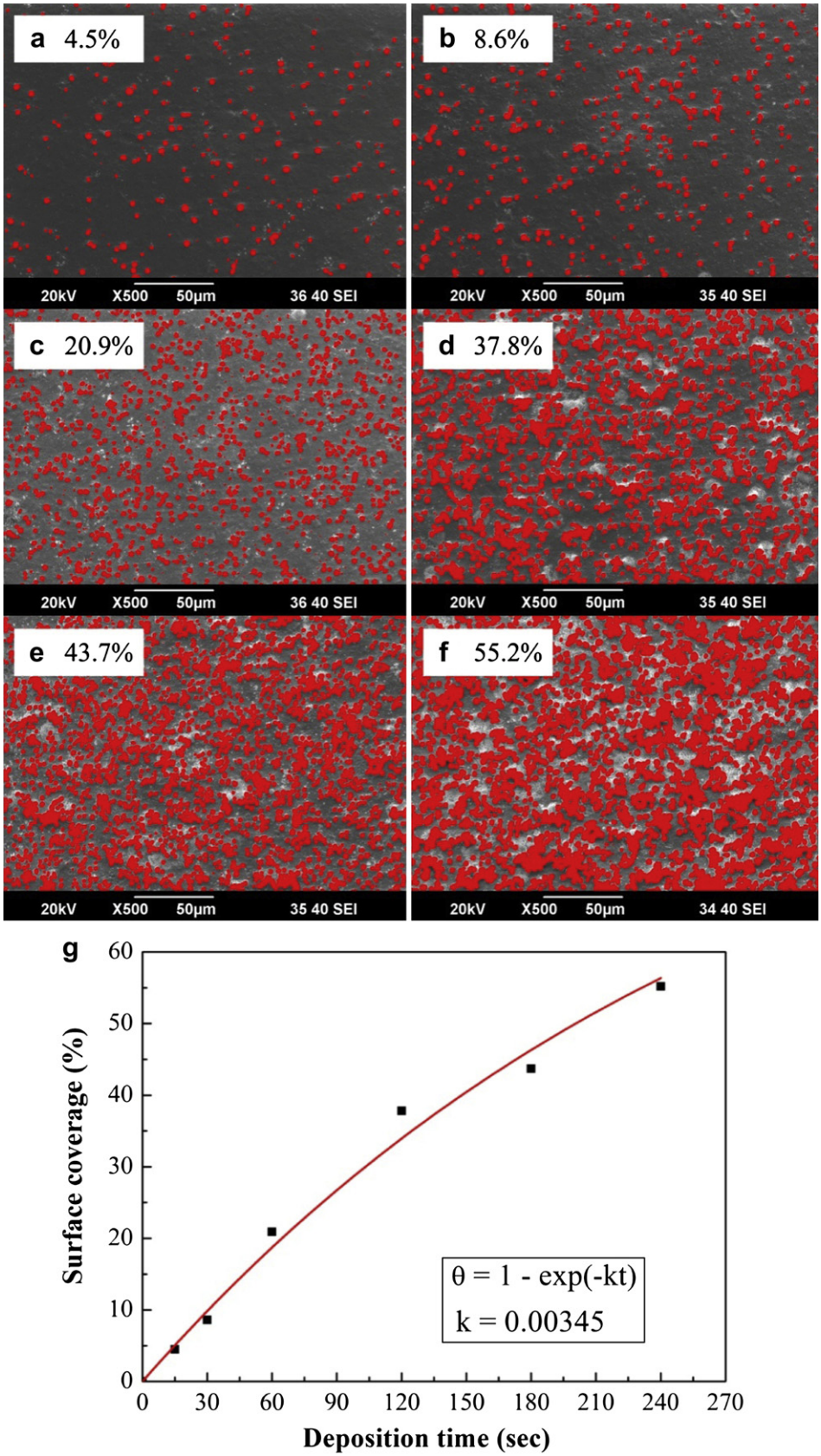


**Fig. 4.** SEM images showing the surface coverage of the embossing structure by the powder-balls at the deposition time of (a) 15 s, (b) 30 s, (c) 60 s, (d) 120 s, (e) 180 s and (f) 240 s. The painted dots are the images of powder-balls for calculating the surface coverage. (g) is the surface coverage of the powder-ball as a function of the deposition time and the solid line is Langmuir isotherm.

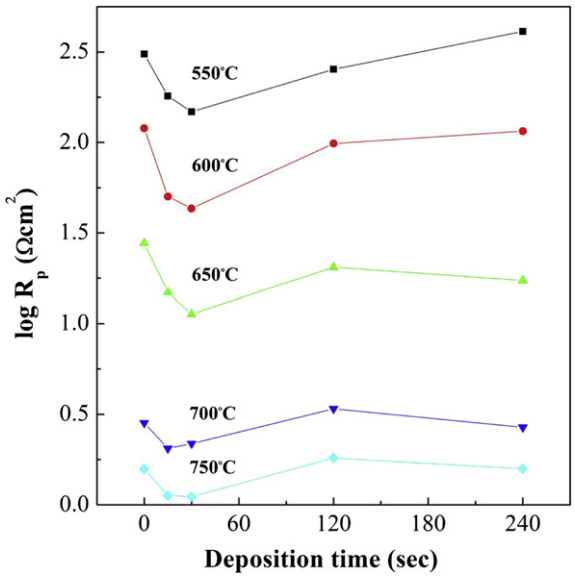


**Fig. 5.** The variation in the polarization resistance with the deposition time of powder-ball.

The temperature dependences of the polarization resistance of the half cell with the optimized deposition time are shown in Fig. 6, where the individual impedance spectra are compared with the one without embossing structure (flat structure). The measured impedance spectra were fitted with an equivalent circuit shown in the inset of Fig. 6(a) ($R_0L_1(R_1CPE_1)(R_2CPE_2)(R_3CPE_3)$) when $R_0$ is ohmic resistance and $L_1$ is inductance and $CPE_1$, $CPE_2$, $CPE_3$ are constant phase elements, and $R_1$, $R_2$, $R_3$ are the polarization resistances of cathodes for high, middle and low frequency range. The polarization resistances of the half cell with embossing structure were reduced by 62.3, 61.5, 38.2, and 34.4% at 600, 650, 700 and 750 °C than that of the flat half cell, respectively. In addition, the $R_1$ among the polarization resistance was significantly decreased by embossing structure as shown in the inset Fig. 6(a) and (b). This result is not in agreement with the studies of modified electrolyte surface morphology reported by Herbstritt et al. [12] and Wang et al. [13]. In these studies, the high frequency arc was not decreased by the modified electrolyte surface morphology. To find out the cause, the variation of impedance spectra as a function of oxygen partial pressure ($PO_2$) was measured. As a result, the $R_1$ is independent of the oxygen partial pressure as presented in Fig. 7(a), and the dependence of $R_1$ on $PO_2$ yields a slope $m = 0.016$ (Fig. 7(b)). The $m$ value can be used to assign a specific arc to the related cathode process, and this almost zero $m$ value means that the arc denoted by $R_1$ caused by oxygen ions transfer at the cathode–electrolyte interface [20–24]. It is reasonable to speculate that the $R_1$ is the resistance at the cathode–electrolyte interface since the $R_1$ is obviously decreased in the sample with the embossing structures. The reason that the reduction in interfacial resistance was not observed in the studied of Herbstritt et al. and Wang et al. may be due to the high cell test temperature. Their impedance measurements were performed at high temperatures (850–950 °C), and, hence, the magnitude of the oxygen ions transfer resistance at the cathode–electrolyte interface seems to be already very small [21,25,26] and no noticeable effect of the modified surface morphology was observed. In contrary, the resistance of cathode–electrolyte interface becomes appreciably

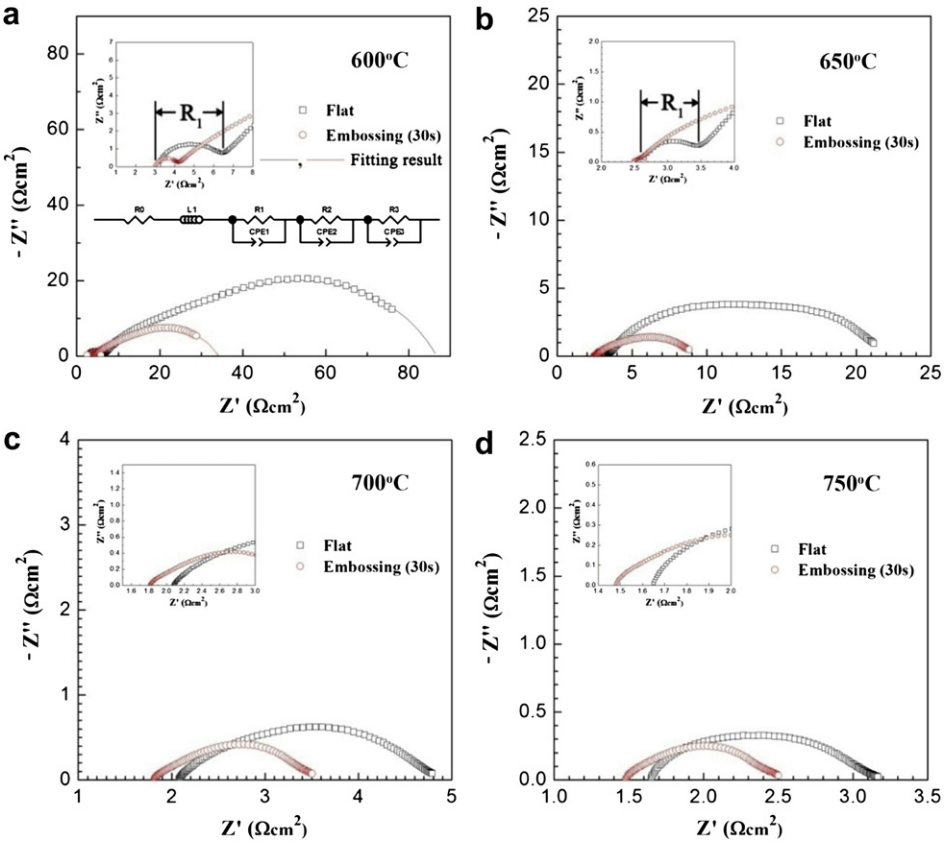


**Fig. 6.** The impedance spectra of the specimen without ('flat') and with deposition of powder-ball for 30 s ('embossing') at various temperatures.

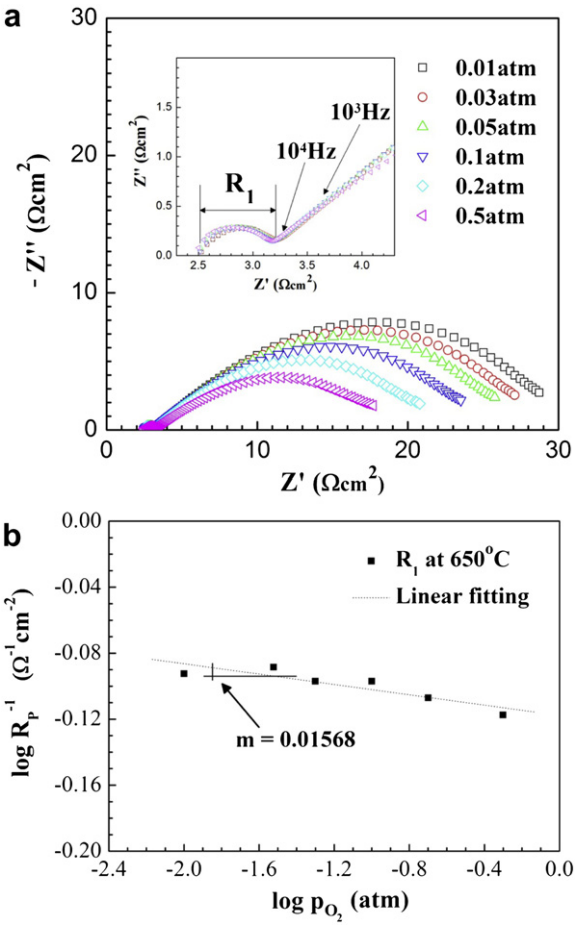


**Fig. 7.** (a) The variation of impedance spectra and (b) dependence of high frequency resistance as a function of oxygen partial pressure at 650 °C for 'flat' half cell.

large at intermediate temperatures, and the embossing structure can reduce this resistance as shown in Fig. 6. Interestingly, the embossing structure reduces not only the $R_1$ but also whole cathode polarization resistances. It means that the cathode–electrolyte interface resistance is important to the whole cathode performance and the embossing structure is very effective to increase the cathode efficiency. For this reason, the beneficial

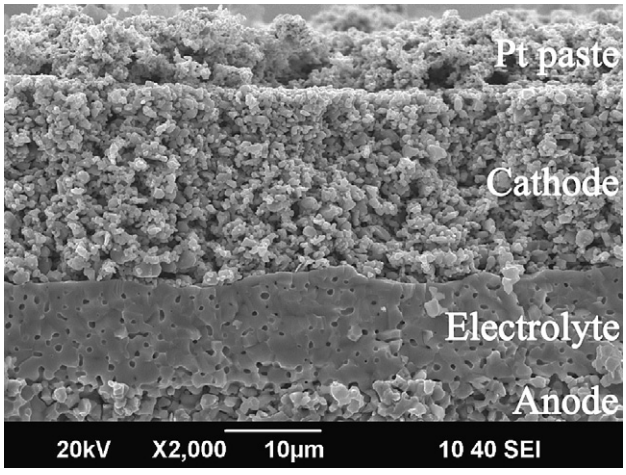


**Fig. 8.** Cross-sectional SEM images of a single cell fabricated by ESSD method.

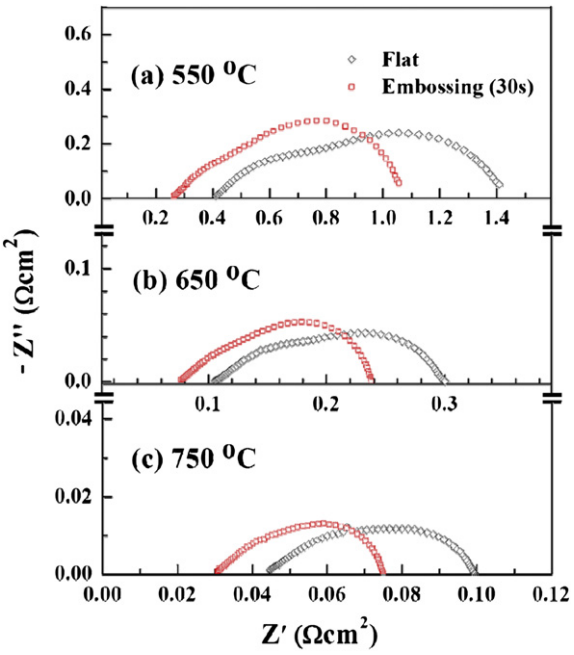


**Fig. 9.** Impedance spectra of the tested cell measured under open current conditions at different temperatures with humidified $H_2$ as a fuel and air as an oxidant, respectively.

effect of the embossing structure is more prominent at relatively low temperature.

### 3.2. Performance enhancement in the single cells

The single cell with the optimized embossing structure determined in the half cell study was fabricated by the ESSD. A cross-sectional microstructure of the single cell after performance evaluation is shown in Fig. 8. Although some closed pores are found in

**Table 1**
Summary of the performances of 'flat' and 'embossing' single cells. The increment is calculated by (Embossing/Flat − 1) × 100.

| Temp./°C | OCV/V | | | Power density/mW cm$^{-2}$ | | |
|---|---|---|---|---|---|---|
| | Flat | Embossing | Increasing rate | Flat | Embossing | Increasing rate |
| 550 | 0.8144 | 0.8552 | +5.01% | 171 | 232 | +33.67% |
| 600 | 0.7987 | 0.8371 | +4.81% | 335 | 448 | +33.73% |
| 650 | 0.7815 | 0.8149 | +4.27% | 590 | 735 | +24.58% |
| 700 | 0.7577 | 0.7847 | +3.56% | 891 | 1030 | +15.47% |
| 750 | 0.7261 | 0.7448 | +2.58% | 1056 | 1187 | +12.41% |

**Table 2**
Numerical values of the ohmic resistances ($R_o$) and polarization resistances ($R_p$) of the tested single cell estimated from impedance spectroscopy under open circuit conditions at different temperatures.

| Temp./°C | | R (Ω cm$^2$) | | |
|---|---|---|---|---|
| | | $R_o$ | $R_p$ | $R_{Total}$ |
| 550 | Flat | 0.411 | 0.99 | 1.401 |
| | Embossing (30 s) | 0.26 | 0.79 | 1.05 |
| 600 | Flat | 0.187 | 0.452 | 0.639 |
| | Embossing (30 s) | 0.130 | 0.343 | 0.473 |
| 650 | Flat | 0.106 | 0.194 | 0.3 |
| | Embossing (30 s) | 0.077 | 0.160 | 0.237 |
| 700 | Flat | 0.063 | 0.101 | 0.164 |
| | Embossing (30 s) | 0.046 | 0.084 | 0.13 |
| 750 | Flat | 0.044 | 0.056 | 0.1 |
| | Embossing (30 s) | 0.031 | 0.044 | 0.075 |

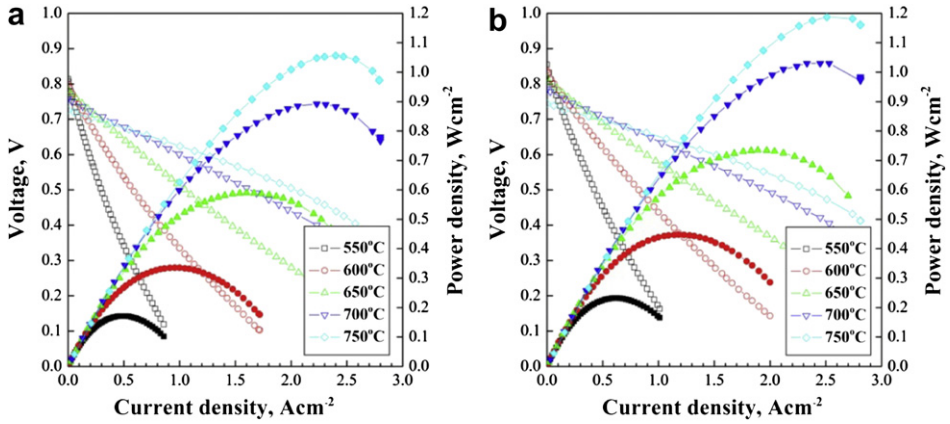


**Fig. 10.** *I–V* and *I–P* characteristics of (a) 'flat' and (b) 'embossing' single cell in the temperatures range from 550 to 750 °C.

the 10 μm thick electrolyte, no serious problem was found in maintaining open circuit voltage (OCV). A uniformly porous cathode film was fabricated and the thickness was about 20 μm. The deposition time for the electrolyte and cathode layer was each 20 min, which are remarkably shorter than the conventional cell fabrication techniques.

The electrochemical impedance spectra of the single cell measured under open circuit conditions are shown in Fig. 9. The intercept with the real axis high frequencies represents the ohmic resistance ($R_o$) of the cell, which includes ionic resistance of the electrolyte, whereas the difference between the high frequency and the low frequency intercept with the real axis represents the polarization resistance ($R_p$) of the single cell. The detailed values for the $R_o$, $R_p$ and $R_{Total}$ were summarized at Table 2. The measured $R_o$ and $R_p$ of the single cell with the embossing structure were lower than that of the cell without the modification at all temperature range. These improved electrochemical properties contributed to the single cell performance. *I–V* and power density curves for the single cells with and without the embossing structure are shown in Fig. 10. The exact measured values of OCV and the maximum power densities are summarized in Table 1. The OCV value of embossing single cell was slightly higher than the flat single cell. This difference is believed to be caused by the change of electrolyte thickness. In the literature, it is reported that thin GDC electrolyte shows a reduced OCV due to electronic conduction and the OCV increase when increasing GDC electrolyte thickness [27,28]. Thus, it is reasonable to assume that the embossing structures slightly increase the thickness of electrolyte and, hence, the suppressed electronic conduction throughout the electrolyte results in the increased OCV. As summarized in Table 1, the maximum power densities of embossing single cell were increased by 12.41%, 15.47%, 24.58%, 33.73% and 35.67% at 750, 700, 650, 600 and 550 °C compared with the flat single cell. Although it has been pointed out in the above mentioned literature [27,28] that the thicker electrolyte generally reduced the power density because of the increased ohmic resistance of the electrolytes, the embossing single cell in this study showed the higher power densities than the flat single cell. This remarkable improvement in the power density seems to be caused by the combined effect of increased OCV value and the reduced interfacial ohmic resistance. Similarly to the variation in the polarization resistance of the cathode, this remarkable performance enhancement was more prominent at relatively lower operating temperature. Consequently, the embossing structure fabricated in this study is expected to be more effective and beneficial in the IT-SOFCs (Fig. 10).

## 4. Conclusions

The powder-balls generation phenomenon by electrostatic slurry spray deposition (ESSD) is first reported in this study, and the embossing structure utilizing this powder-ball was successfully fabricated on GDC electrolyte layer. Especially, the sufficient amount of powder-ball could be rapidly and conveniently deposited on GDC electrolyte in tens of seconds by ESSD method. The cathode polarization resistance in half cell was dramatically reduced by 62.3% at 600 °C by embossing structure covering only 8.6% of the electrolyte surface. In addition, the OCV values were also slightly increased by 2–5% and this is because the embossing structure increases the thickness of GDC electrolyte. The maximum power density of single cell was also increased from 1.056 and 0.171 to 1.187 (+12.41%) and 0.232 W $cm^{-2}$ (+35.67%) at 750 and 550 °C, respectively. In conclusion, the embossing structure applied in the cathode–electrolyte interface produced desirable performance enhancement of the SOFCs in all temperature range from 550 °C to 750 °C, and this enhancement is found to be especially suitable to intermediate-temperature SOFCs.

## Acknowledgments

This work is the outcome of a Manpower Development Program for Energy supported by the Ministry of Knowledge Economy (MKE) and also, supported by Solid oxide fuel cell of New & Renewable Energy R&D program (20093021030010) under the Korea Ministry of Knowledge Economy (MKE).

## References

[1] S. Souza, S.J. Visco, C. Lutgard, D. Jonghe, Solid State Ionics 98 (1997) 57–61.
[2] Y.J. Leng, S.H. Chan, S.P. Jiang, K.A. Khor, Solid State Ionics 170 (2004) 9–15.
[3] X. Zhang, M. Robertson, S. Yick, C. Deĉes-Petit, E. Styles, W. Qu, Y. Xie, R. Hui, J. Roller, O. Kesler, R. Maric, D. Ghosh, J. Power Sources 160 (2006) 1211–1216.
[4] K. Xie, Q. Ma, B. Lin, Y. Jiang, J. Gao, X. Liu, G. Meng, J. Power Sources 170 (2007) 38–41.
[5] C.G. Fonseca, R.M.F. Basaglia, M.C. Brant, T. Matencio, R.Z. Domingues, Powder Technol. 192 (2009) 352–358.
[6] B. Lin, J. Chen, Y. Ling, X. Zhang, Y. Jiang, L. Zhao, X. Liu, G. Meng, J. Power Sources 195 (2010) 1624–1629.
[7] T. Suzuki, S. Sugihara, T. Yamaguchi, H. Sumi, K. Hamamoto, Y. Fujishiro, Electrochem. Commun. 13 (2011) 959–962.
[8] H. Song, S. Lee, D. Lee, H. Kim, S. Hyun, J. Kim, J. Moon, J. Power Sources 195 (2010) 2628–2632.
[9] Y.W. Ju, T. Inagaki, S. Ida, T. Ishihara, J. Electrochem. Soc. 158 (7) (2011) B825–B830.
[10] I. Park, J. Im, J. Choi, J. Ahn, D. Shin, Solid State Ionics 184 (2011) 35–38.

[11] J. McCoppin, D. Younga, T. Reitz, A. Maleszewski, S. Mukhopadhyay, J. Power Sources 196 (2011) 3761–3765.
[12] D. Herbstritt, A. Weber, E. Ivers-Tiffee, J. Eur. Ceram. Soc. 21 (2001) 1813–1816.
[13] X.M. Wang, C.J. Li, C.X. Li, G.J. Yang, J. Thermal Spray Technol. 19 (2010) 311–316.
[14] A. Konno, H. Iwai, K. Inuyama, A. Kuroyanagi, M. Saito, H. Yoshida, K. Kodani, K. Yoshikat, J. Power Sources 196 (2011) 98–109.
[15] I. Park, J. Ahn, J. Im, J. Choi, D. Shin, Ceram. Int. 38S (2012) S481–S484.
[16] J. Choi, J. Im, I. Park, D. Shin, Ceram. Int. 38S (2012) S489–S492.
[17] A. Jaworek, J. Mater. Sci. 42 (2007) 266–297.
[18] R.P.A. Hartman, J.P. Borra, D.J. Brunner, J.C.M. Marijnissen, B. Scarlett, J. Electrostat. 47 (1999) 144–148.
[19] A. Jaworek, A.T. Sobczyk, J. Electrostat. 66 (2008) 197–219.
[20] M.J. Escudero, A. Aguadero, J.A. Alonso, L. Daza, J. Electroanal. Chem. 611 (2007) 115–121.
[21] X. Xu, Z. Jiang, X. Fan, C. Xia, Solid State Ionics 177 (2006) 2113–2116.
[22] S.W. Baek, J. Bae, Y. Yoo, J. Power Sources 193 (2009) 437–444.
[23] Y. Li, R. Gemmen, X. Liu, J. Power Sources 195 (2010) 3354–3362.
[24] R. Amin, B. Kenney, K. Karan, J. Electrochem. Soc. 158 (2011) B1076–B1082.
[25] X. Xu, C. Xia, G. Xiao, D. Peng, Solid State Ionics 176 (2005) 1513–1520.
[26] A.A. Solov'ev, N.S. Sochugov, A.V. Shipilova, K.B. Efimova, A.E. Tumashevskaya, Elektrokhimiya 47 (2011) 524–533.
[27] C. Ding, H. Lin, K. Sato, K. Amezawa, T. Kawada, J. Mizusaki, T. Hashida, J. Power Sources 195 (2010) 5490–5493.
[28] K.L. Duncan, K.T. Lee, E.D. Wachsman, J. Power Sources 196 (2011) 2450–2452.